Nuclear Materials and Energy 37 (2023) 101527

Contents lists available at ScienceDirect

Nuclear Materials and Energy

journal homepage: www.elsevier.com/locate/nme

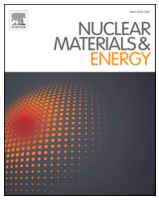

Compatibility of EUROFER97 and lead–lithium eutectic

Kateryna Khanchych *, Carsten Schroer

Karlsruhe Institute of Technology, Institute for Applied Materials – Applied Materials Physics (IAM-AWP), Hermann-von-Helmholtz-Platz 1, 76344 Eggenstein-Leopoldshafen, Germany

ARTICLE INFO

Keywords:
EUROFER97
Pb–16Li
Dissolution
Solubility
Diffusivity
Mechanical properties

ABSTRACT

Information as concerning the compatibility of EUROFER97, or other martensitic steels, and liquid lead–lithium eutectic is collected and evaluated. The best part addresses dissolution caused by the liquid metal, whereas data on the effect on characteristic mechanical properties of the steel are scarce, and even scarcer for the simultaneous influence of neutron irradiation. The latter must be taken into account for application to thermonuclear fusion, as well as, in case of magnetic confinement of the fusion fuel, the acceleration of EUROFER dissolution in the presence of a magnetic field. A degradation of mechanical properties of the steel caused by the liquid metal manifests itself in a loss of ductility, which requires an incubation period just as the dissolution process in the absence of a mechanical load on the material. As a basis for discussing the dissolution phenomena observed, data on the solubility and diffusivity of the major elements in EUROFER is reviewed and dissolution theory briefly repeated.

1. Introduction

In thermonuclear fusion reactors, the functional and structural materials employed will, inter alia, face an unprecedented irradiation load, notably caused by the high-energy neutrons released by the fusion reaction. One of the anticipated responses is the transmutation of the constituent parts as well as impurity elements in such materials into radioactive isotopes, which later on will significantly impact the requirements for controlled handling, storage and disposal of the reactor components at the end of their lifetime. Accordingly, a low-activation strategy is being pursued, especially for the structural materials that will serve as the vacuum boundary of the reactor main chamber, containment of the breeding blanket, where the tritium for maintaining the fusion reaction is produced and heat transferred onto a coolant loop, or the piping for coolant and vacuum lines. As for steels, this has led to the development of reduced-activation ferritic-martensitic steels (RAFM) from the conventional 9Cr–1Mo grades, in which strongly activating elements such as Mo, Nb, Ni, Cu or N are substituted as far as possible by equivalent non- or less activating elements like W, V or Ta. The European RAFM steel is EUROFER97, specified regarding concentration of major and minor elements [1] as listed in Table 1. More background as to the development of EUROFER97, its microstructure or numbers of mechanical properties have been published elsewhere [1].

In the breeding blanket, structural materials, i.e., RAFM steel, come into contact with the tritium-breeding material as well as the coolant that extracts heat from the reactor. A number of blanket concepts are currently being developed in parallel, some of which make use of eutectic lead–lithium (Pb–16Li) as the tritium breeder, or coolant, or both [2]. This raises the question for the persistence of RAFM steel in contact with the liquid alloy, under the conditions in the breeding blanket, not only regarding potential solution of the constituent elements but also degradation of mechanical properties of the steel [3]. Even in the case that, e.g., the tritium balance of the reactor renders a permeation barrier on blanket components generally mandatory, which will effectively separate Pb–16Li and steel, their interaction nevertheless remains of some importance where such coating locally fails, or for surfaces that may or, finally, must stay uncoated.

In the following, fundamental aspects of the interaction of steels with liquid metals in general, and Pb–16Li in particular, are introduced and discussed, along with considerations regarding mass transport in the liquid phase. Available information on the solubility and diffusivity in Pb–16Li of relevant metallic elements is presented and evaluated, and used later for analyzing experimental observations on the response of EUROFER and other RAFM or martensitic steels in contact with this liquid metal.

* Corresponding author.
E-mail address: kateryna.khanchych@kit.edu (K. Khanchych).

https://doi.org/10.1016/j.nme.2023.101527
Received 3 July 2023; Received in revised form 11 September 2023; Accepted 26 September 2023
Available online 27 September 2023

Table 1
Chemical composition (% by mass) as specified for EUROFER97 (Balance Fe) [1].

Cr	W	Mn	V	Ta	C	N	Ti	Si	P	S	Cu	Nb	Ni	Mo	B
8.5–9.5	1.0–1.2	0.20–0.60	0.15–0.25	0.10–0.10	0.10–0.12	0.015–0.045	<0.01	<0.05	<0.005	<0.005	<0.005	<0.001	<0.005	<0.005	<0.001

2. Liquid-metal corrosion

In the broadest sense, liquid–metal corrosion may be understood as the degradation of a solid material caused by direct interaction with the principal constituent parts of a liquid metal. Such degradation can take various forms, and is often observed as a measurable recession of the dimensions of the unaffected part of the material. However, more subtle effects of interaction may possibly occur, accessible in this case only with advanced, not routinely applied techniques of material analysis [4] or indirectly found as a change in specific, e.g., mechanical properties of the material [5,6].

Fig. 1 gives an overview of primarily physical processes that are likely to, partly only possibly occur if a pure solid metal with pristine surface is brought into contact with a liquid metal. As for the very first interactions (Fig. 1a), it is assumed that the solid surface adsorbs atoms of liquid metal. In connection with adsorption, grain boundaries intersecting with the solid surface may recede so as to minimize surface energy, and also other near-surface defects might show specific responses. At the latest after significant penetration of atoms of the liquid metal along grain boundaries, a detrimental effect on mechanical performance can be expected [7]. Absorption of atoms from the liquid into the grains of the solid phase may also occur, though limited by relatively low saturation concentration and diffusivity in the solid.

Interactions mentioned so far are unlikely to result in a clear change in position of the solid-metal surface, whereas mass transfer from solid to liquid (Fig. 1b), i.e., solution of the solid, generally involves a recession of this surface. Such solution is limited only by global saturation of the liquid metal with the transferring atoms, which, however, will not occur or at least be significantly delayed, if the latter find ways of reprecipitating, e.g., on another, cooler solid surface that is in contact with the liquid metal. This circumstance is understood as corrosion mass transfer (from hot to cold) [8], often termed mass transfer corrosion. Certain couples of solid and liquid metal form ordered solid solutions, or intermetallic phases, after local saturation of either the solid or liquid, depending on the dominant direction of atom transfer across the solid/liquid interface, along with the relevant saturation concentrations. If the intermetallic evolves into a surface layer on the original metal, as indicated in Fig. 1c, its interface with the liquid metal constitutes the new solid/liquid interface. The surface of original metal that remains unaffected by the interaction with the liquid metal generally recedes. The intermetallic layer, or any other surface layer, naturally impacts the rate of further mass transfer in both directions.

The phenomena, types of attack [9] or corrosion modes observed in the solid after interacting with the liquid metal may be various, partly originating from the fact that the solid metal under consideration was an alloy rather than pure, a surface layer, however composed, already existed before first contact with the liquid, or the liquid metal carried impurities, notably non-metals such as oxygen, that interfered with the fundamental interactions. An overview based upon earlier categorization [9] is tried with the aid of Table 2, additionally identifying the elemental processes involved. Corrosion mass transfer (Row 2 of this table) is understood here in the most general manner, as a transfer via the liquid metal from the solid metal or alloy under consideration into another solid phase, driven not only by a temperature gradient in the system but also by concentration (chemical activity) gradients or other [9]. The decisive subprocess is reprecipitation, allowing for complete consumption of constituent elements in the original material even at rather low saturation concentration or small liquid–metal volume available. Reprecipitation may occur in the form of pure metal, as a constituent part of an alloy, intermetallic phase or non-metallic compound, e.g., oxide. In this spirit, the second mechanism of selective leaching of certain elements from alloys (Row 3.2 of Table 2) [10] can be regarded as a special case of corrosion mass transfer, involving only short-distance transport (diffusion), without intermittent transfer to the bulk of the liquid metal. Absorption of atoms from the liquid into the solid (Row 5) refers to both the principal constituents of the liquid metal

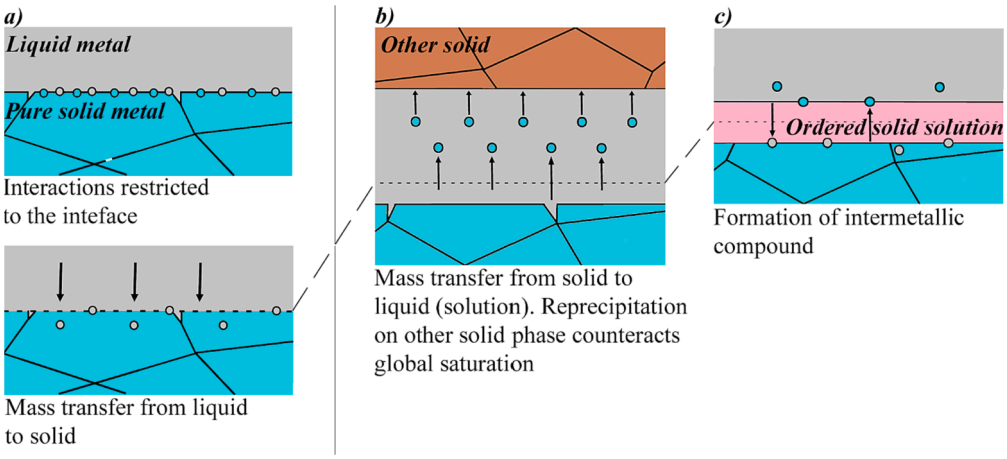

Fig. 1. Illustration of interactions that occur between solid metal with pristine surface (pure or polycrystalline) and liquid metal, which are primarily of physical nature: (a) Processes resulting in degradation of mechanical properties rather than recession of the metal surface and (b,c) processes likely to involve noticeable surface recession or metal loss. Dashed lines indicate the original position of the solid surface.

Table 2
Phenomena and elemental processes involved in liquid–metal corrosion of pure metals and alloys.

	Phenomenon	Elemental processes
1	Solution of the solid in the liquid metal, non-selective in the case of alloys	Atom transfer from solid to liquid across the solid/liquid interface. Diffusion in concentration gradient, into the bulk of the liquid metal. Convective mass transport in dynamic liquid phase.
2	Corrosion mass transfer	Solution plus atom transfer from liquid to solid of previously dissolved element(s) to another solid phase (reprecipitation). Diffusion in concentration gradient, from the bulk of the liquid metal towards the other solid phase.
3.1	Selective leaching in alloys (type I)	Solid-to-liquid atom transfer not in proportion to the original alloy composition. Counterdiffusion of elements depleting and enriching, respectively, in the near-surface alloy. Diffusion of atoms transferred to the liquid metal.
3.2	Selective leaching in alloys (type II)	Atom transfer across solid/liquid interface in proportion to the alloy composition. Reprecipitation of certain elements after short-range diffusion, diffusion of others directly into the bulk of the liquid metal. Subsequent solution of intermittently reprecipitated metal (alloy).
4	Faceting	Solution/reprecipitation with rates depending on crystallographic orientation. Or Surface diffusion of atoms of the solid.
5	Absorption of atoms from the liquid into the solid metal or alloy	Adsorption at the solid surface. Atom transfer across the solid/liquid interface. Solid-state diffusion, possibly precipitation.
6	Surface-layer formation	Additional solid-to-solid atom transfer(s) for layer growth or solution through the layer. Additional solid-state diffusion across layer(s).

and impurities, i.e., also to non-metals. The principal difference between surface-layer formation (Row 6) and corrosion mass transfer as defined above is that atoms from the corroding solid first transfer to the other solid phase involved, before transfer to the liquid metal is possible. Again, such a surface layer can be an intermetallic phase or a non-metallic compound with impurity in either the liquid or solid metal.

3. Mass transport in the liquid phase

Solution of a pure solid metal in a liquid metal can be considered as a two-stage, heterogeneous reaction that firstly, consists of atom transfer across the solid/liquid interface. The bonds of atoms in the crystal lattice of the solid metal must break, and new links to atoms in the liquid metal form. As typical for thermochemical process, the reverse reaction also takes place, however, initially with much lower rate. The rate of the reverse reaction increases with increasing accumulation in the liquid of the atoms transferring from the solid, until, at saturation of the liquid, notably at the solid/liquid interface, atom transfer to the liquid and reprecipitation occur with same rates (Nernst-Brunner theory). The net transfer of atoms between the solid and the liquid is zero at this point in time as well as in the following, whereas individual atoms are still exchanged across the solid/liquid interface. In the case of single-phase alloys, the rate of transfer from solid to liquid of atoms of the individual alloying elements and also their saturation concentrations in the liquid are a function of the concentrations in the solid, at the solid/liquid interface. The second stage of solution is transport from the solid/liquid interface into the volume of the liquid metal, diffusion, supported by convection in a moving liquid. The combination of these two processes is called convective diffusion [11].

In isothermal convective diffusion in the absence of force fields, the total flux $\vec{j}$ of a solute generally is a vector given by

$$\vec{j} = c\vec{v} - D\nabla c, \tag{1}$$

where c – molar concentration of the solute, D – diffusion coefficient, $\vec{v}$ –flow velocity. The first term corresponds to convection, the second to diffusion in a concentration gradient. The space and time dependence of the concentration follows as

$$\frac{\partial c}{\partial t} + (\vec{v}\nabla)c = D\Delta c \tag{2}$$

(incompressible liquid). Eq. (2), representing a balance of matter, is essentially similar to the Navier-Stokes equation for the conservation of momentum. If $\frac{\partial c}{\partial t} = 0$ (stationary or steady state)

$$(\vec{v}\,\nabla)c = D\Delta c, \tag{3}$$

whereas Fick's second law results for $\vec{v} = 0$ (static liquid):

$$\frac{\partial c}{\partial t} = D\Delta c. \tag{4}$$

Rewriting Eq. (3) in dimensionless form by introducing a characteristic length l_0 along which the main change in concentration occurs, the characteristic velocity (the average velocity in the bulk of the liquid) u_0, as well as the concentration c_0 in the bulk of the liquid gives

$$V_x\frac{\partial C}{\partial X} + V_y\frac{\partial C}{\partial Y} + V_z\frac{\partial C}{\partial Z} = \frac{D}{u_0 l_0}\left(\frac{\partial^2 C}{\partial X^2} + \frac{\partial^2 C}{\partial Y^2} + \frac{\partial^2 C}{\partial Z^2}\right) \tag{5}$$

with dimensionless space coordinates $X = \frac{x}{l_0}, Y = \frac{y}{l_0}, Z = \frac{z}{l_0}$, components of the dimensionless velocity vector $V_x = \frac{v_x}{u_0}, V_y = \frac{v_y}{u_0}, V_z = \frac{v_z}{u_0}$ and dimensionless concentration $C = \frac{c}{c_0}$. The factor before the brackets on the right-hand side is the inverse Péclet number defined as $Pe = \frac{u_0 l_0}{D}$, which characterizes the ratio of convective and diffusive mass transport. It plays for convective diffusion the same role as the Reynolds number $Re = \frac{u_0 l_0}{\nu}$ (with ν – kinematic viscosity) for fluid flow, which characterizes the ratio of inertial force to viscous friction force. For small *Pe*, the share of convection is small, and the concentration distribution determined mainly by molecular diffusion.

The ratio of *Pe* and *Re* is the Schmidt number $Sc = \frac{\nu}{D}$, which depends neither on flow velocity nor on a characteristic length but only on properties of the liquid that are relevant to transport of momentum and matter by purely molecular mechanisms. For liquids, in contrast to gases, *Sc* is large so that even at low *Re* (e.g. 10^{-2}) $Sc > 1$. This means for Reynolds numbers usually encountered in practice, convective mass transport clearly prevails over diffusion [11]. In other words, the diffusion boundary layer at the surface of a solid dissolving into a moving liquid, across which the concentration of transferred atoms decreases from the concentration at the solid/liquid interface to that in the bulk of the liquid, is relatively thin, especially thinner than the corresponding hydrodynamic boundary layer because of $Pe \gg Re$.

At given thickness δ of the diffusion boundary layer, the stationary concentration gradient perpendicular to the dissolving solid surface may be estimated. It follows from the difference of stationary concentrations at the solid/liquid interface ($c_{s/l}$) and in the bulk of the liquid (c), i.e., the quotient of this concentration difference and δ. If transport, notably diffusion, rather than atom transfer is the rate-determining step in the solution process, solution rate is

$$\frac{dn}{dt} = \frac{D}{\delta}\left(c_{s/l} - c\right)\cdot A, \tag{6}$$

where $\frac{dn}{dt}$ – number of moles transferred per unit time; A – surface area of the dissolving solid. $c_{s/l}$ approaches the saturation concentration. δ is a function of properties of the liquid and characteristic velocity [11], e.g.

$$\delta \approx D^{\frac{1}{6}}\nu^{\frac{1}{6}}\sqrt{\frac{x}{u_0}}. \tag{7}$$

Qualitatively, it makes no difference whether the liquid or the dissolving solid is in movement. For example, for a rotating flat sample [12], δ is

$$\delta = 1.61 D^{\frac{1}{3}}\nu^{\frac{1}{6}}\omega^{-\frac{1}{2}}, \tag{8}$$

where ω denotes the angular speed. It should be noted that diffusion coefficients depend not only on the liquid but also the type of dissolving atoms, i.e., the thickness of the diffusion layer may differ for individual elements dissolving from the same alloy.

4. Solution of metals in eutectic lead–lithium

Lead is a relatively easy-to-alloy metal, which has a significant dissolving power with respect to a number of metallic elements, with tendency to forming intermetallic phases. Metals that are highly soluble in lead include alkali and alkaline earth metals, transition metals of Groups 3 and 4 of the periodic table, platinum metals, lanthanides and actinides, as well as some main group elements such as Sn, Sb or Bi. Lithium is also capable of dissolving a number of metals and forms intermetallic compounds with some of them [13]. Thermodynamic data [14] suggests only weak tendency to dissolving transition metals of Groups 4–7.

The Pb–Li system is an example of miscibility and formation of compounds between lead and alkali metals. The properties of the liquid alloy are mainly governed by the properties of the main component, i.e., Pb in the eutectic with 16 % (by mole) Li. The chemical activity of lithium in this alloy is significantly reduced in comparison to pure Li [15]. Though the capacity of lithium to dissolve metals is much lower than that of lead, the solubility of some metals is higher in liquid Pb–Li alloys than in pure liquid Pb [16]. Metals that are difficult to dissolve in two low-melting metals are likely to show low solubility also in the eutectic alloy, similar to findings for non-metals [14].

In the following subsections, available data on solubility and diffusivity in Pb–16Li of metals relevant to EUROFER97 is presented and discussed. Furthermore, dissolved oxygen and stability of oxides are addressed, and how they may potentially influence the solution process. Where necessary, published solubility data is converted into μg/g and logarithmic equations representing solubility as a function of temperature transcribed to $\log_{10}$. As the eutectic composition was formerly assumed at 17 % Li, data published for Pb–17Li is considered applicable also to Pb–16Li.

4.1. Iron solubility

The solubility of iron in Pb–16Li is estimated by Barker and Sample [17] from the equilibrium concentration (saturation) establishing in a long-term immersion experiment performed on Type 316 steel at 450 °C. With calculated Fe activity in the steel and observed saturation concentration of 0.68 and 20 μg/g, respectively, observed Fe solubility at 450 °C is 30 μg/g. This preliminary [17] value is by 25 % lower than resulting from

$$\log_{10} S_{Fe} = 2.524 - 655.0/T \tag{9}$$

(S_{Fe} – Fe solubility in μg/g, T – temperature in K) as reported by Coen and Sample [18] for Fe solubility in Pb–16Li as a function of temperature, for an unspecified temperature range.

Borgstedt and Feuerstein [19] estimate 0.0449 and 0.242 μg/g (mole fraction 1.41×10^{-7} and 7.6×10^{-7}, respectively) at 500 and 550 °C, respectively, from corrosion tests on steels in turbulent flow, which suggests a temperature dependence of

$$\log_{10} S_{Fe} = 10.74 - 9345/T \tag{10}$$

From dissolving Fe coupons in static Pb–16Li at 500 and 600 °C, Feuerstein et al. [20] find

$$\log_{10} S_{Fe} = 2.15 - 1864/T \tag{11}$$

(S_{Fe} – Fe solubility in μg/g, T – temperature in K). While the parameter values in the inferred dependences on temperature clearly differ, Fe solubility at same experimental temperature (500 °C) is within about one order of magnitude. According to these measurements, Fe solubility in Pb–16Li is by two to three orders of magnitude lower than predicted by Eq. (9), and close to that in pure Pb [21]. The latter complies with the view Kondo et al. [22] obtained from corrosion studies on RAFM steel in Pb–Li alloys with varying Li content, though their approach of estimating solubility in the liquid alloy from the molar fraction of Pb and solubility in pure Pb seems to lack general applicability.

Alternatively to the actual measurement, Lyublinski et al. [23] calculate the solubility of transition metals in low-melting metals with the aid of the Miedema model [24]. From the plots presented in the

respective paper, Fe solubility in Pb–16Li follows as

$$\log_{10} S_{Fe} = 5.276 - 4608/T \quad (12)$$

(S_{Fe} – Fe solubility in μg/g, T – temperature in K), which fairly well agrees with the data reported by Borgstedt and Feuerstein [19,20] (Fig. 2). This, finally, makes Fe solubility of same order as in pure Pb appear more reliable than the significantly higher numbers reported elsewhere [17,18]. Nevertheless, the scarce and partly only indirectly determined (e.g., from solution of steels or observed solution rates) data available for Fe solubility in Pb–16Li gives room for speculating about reliability, and leaves much to the judgement of the user of such data [25]. It should be noted that Lyublinski et al. [23] also address oxygen dissolved in Pb–16Li in their calculations, arriving at the conclusion that about 3 μg/g do not exert remarkable influence on the saturation concentration of Fe.

4.2. Chromium solubility

96 data points for Cr solubility in Pb-16Li obtained by Barker and Sample [17] in the temperature range from 257 to 455 °C are within 1 to 10 μg/g rather than show an easy trend as a function of temperature, which, as stated by the authors, may be connected to oxygen dissolved in the liquid alloy. Coen and Sample [18] report 10 μg/g also at 600 °C. This suggests 10 times higher Cr solubility in comparison with pure lead, if data provided by Alden et al. [26] is extrapolated to 600 °C. Simon et al. [12] equally deduce 10 μg/g for Cr solubility in Pb–16Li from corrosion experiments on two Fe-Cr steels (10.6 and 25.4 % (by mass) Cr, respectively) at 440 °C and 500 °C. Observing selective leaching of neither Cr nor Fe in ferritic steels with 9–12 % Cr during exposure to Pb–16Li, Borgstedt and Feuerstein [19] suppose that Cr solubility is unlikely to differ much from the solubility of Fe (Fig. 2), which would mean Cr solubility order of 1 rather than 10 μg/g. However, other authors actually report near-surface Cr depletion in steels after exposure to Pb–16Li at 440 [27], 480 [28,29], 500 [27,30], 550 [31,32] or 600 °C [22,33], which points to higher Cr solubility in comparison to Fe at the stated temperatures, but, as will become clear later, may as well be the result of oxygen dissolved in the liquid alloy.

As in the case of Fe, Lyublinski et al. [23] calculate the solubility of Cr in Pb–16Li. The temperature dependence as evaluated from plotted results is

$$\log_{10} S_{Cr} = 7.476 - 6454/T \quad (13)$$

(S_{Cr} – Cr solubility in μg/g, T – temperature in K). Similar calculations for pure Pb as the solvent hint at somewhat lower Cr solubility in Pb–16Li than in Pb, at temperature less than about 900 °C. The numbers determined for Cr solubility in Pb–16Li are order of 0.01 to 1 μg/g at temperature in the range from 450 to 600 °C, so not clearly different from Fe solubility in the liquid alloy (Fig. 2). In contrast to solution of Fe, Lyublinski et al. [23] find an influence of dissolved oxygen on the saturation concentration of Cr, which at 3 μg/g dissolved oxygen is somewhat higher than in the absence of oxygen, the more so the lower temperature. This ultimately results from the interaction parameter inferred for dissolved Cr and oxygen (ε^{O}_{Cr}), with absolute value $|\varepsilon^{O}_{Cr}| \gg |\varepsilon^{O}_{Fe}|$, the corresponding value for Fe. Experimental observations on austenitic steel at 600 °C seem to corroborate increasing saturation concentration of Cr with increasing content of dissolved oxygen [33].

Fig. 3 summarizes the findings from the technical literature as regards Cr solubility in Pb–16Li.

4.3. Solubility of minor additions to EUROFER97

As for solubility of Mn, Barker and Sample [17] propose the following linear equation for the temperature range from 258 to 510 °C:

$$\log_{10} S_{Mn} = 6.732 - 2938/T \quad (14)$$

(S_{Mn} – Mn solubility in μg/g, T – temperature in K). The solubility of Mn in Pb–16Li seems to be about half an order of magnitude higher than in pure lead [34] (Fig. 4). It is clearly higher than the solubility of Fe (Fig. 2) or Cr (Fig. 3).

The solubility of V in Pb–16Li deduced by Feuerstein et al. [20] is

$$\log_{10} S_{V} = 4.39 - 3357/T \quad (15)$$

(S_{V} – Mn solubility in μg/g, T – temperature in K). Resulting values (Fig. 4) are comparable with solubility of Fe (Fig. 2) or Cr (Fig. 3).

Feuerstein et al. [20] also report single values for Ta and W solubility in Pb–16Li at 600 °C, namely 0.19 and < 1 μg/g, respectively. Especially W is likely to exhibit very low solubility in Pb alloys in general, as indicated by < 44.4 μg/g (0.005 % by mole) observed for pure Pb at 1200 °C [26].

4.4. Oxygen dissolved in Pb–16Li

Oxygen dissolved in Pb–16Li is not only likely to play a role for the saturation concentration of steel elements as the calculations by Lyublinski et al. [23] suggest, but is also important in respect of the stability of oxides, especially Li-containing ternary oxides such as $LiCrO_2$. With the aid of electrochemical measurements, Barker et al. [35] narrow oxygen solubility down to two equations:

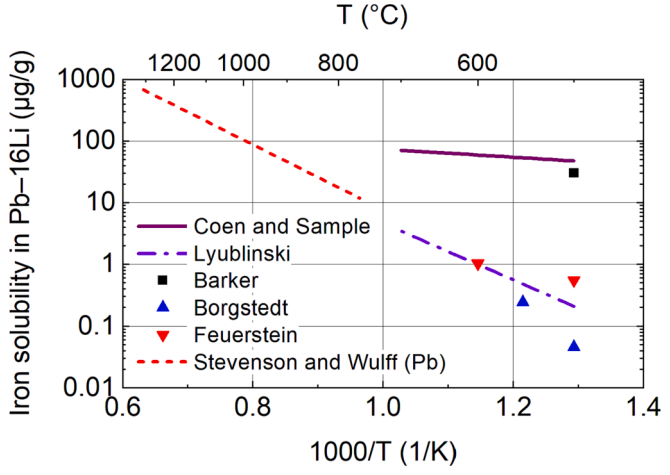

Fig. 2. Summarizing plot of solubility data for Fe in Pb–16Li from different sources [17–21,23].

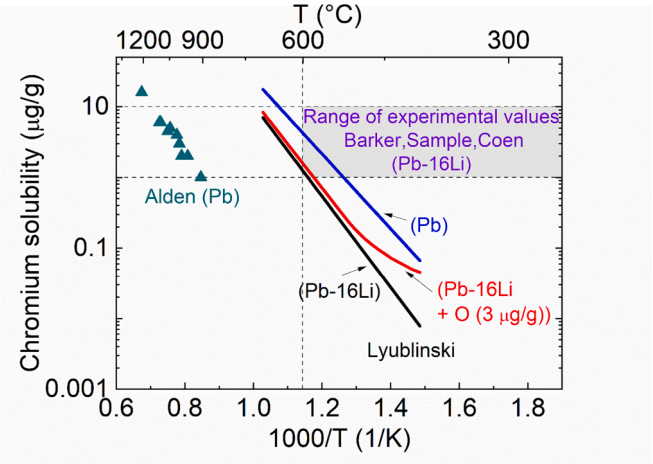

Fig. 3. Solubility of Cr in Pb-16Li and saturation concentration in the presence of dissolved oxygen as found experimentally [17,18] or by calculations [23] in comparison to corresponding data for Pb [26].

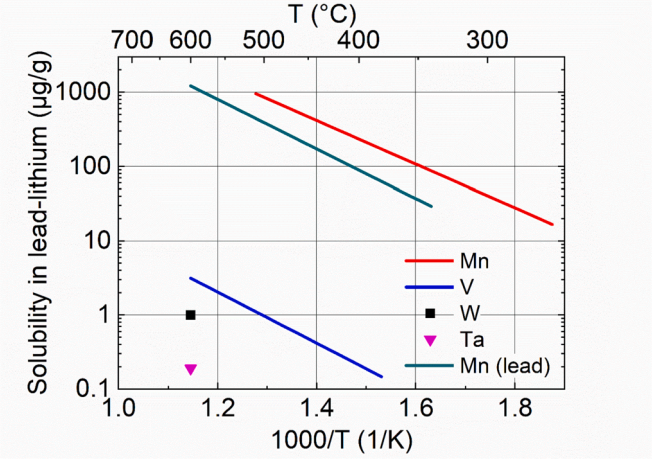

Fig. 4. Solubility data of minor additions to steels in Pb-16Li [17] and Pb [34], respectively.

$$\log_{10} S_O = 2.945 - 4016/T \quad (16)$$

$$\log_{10} S_O = 5.488 - 6145/T \quad (17)$$

The results are in contrast to by several orders of magnitude higher values calculated earlier by Buxbaum [36], who reports

$$\log_{10} S_O = 4.36 - 2380/T \quad (18)$$

(S_O – oxygen solubility in µg/g, T – temperature in K).

For known oxygen solubility and Li activity [15] in Pb–16Li, threshold oxygen concentrations for the stability of oxides may be determined. For Li_2O this naturally is the oxygen solubility. For other oxides such as Cr_2O_3 or $LiCrO_2$ this concentration follows from their standard Gibbs free energy of formation and corresponding data for Li_2O. Fig. 5 exemplifies the results for oxygen solubility according to Eq. (16) (with thermochemical data taken from the database of commercial

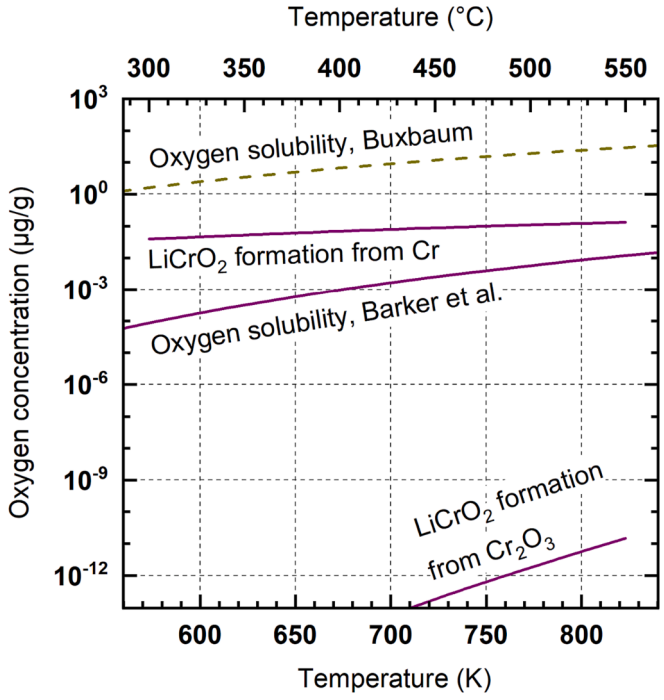

Fig. 5. Oxygen solubility in Pb–16Li as determined by Barker et al. [35] (Eq. (16) and Buxbaum [36] as well as threshold oxygen concentrations for $LiCrO_2$ formation calculated on the basis of oxygen solubility found by Barker et al.

software [37]), which indicate that for formation of $LiCrO_2$ from Li and Cr in Pb–16Li, the concentration of dissolved oxygen must exceed its solubility in the liquid alloy. In other words, this ternary oxide is likely to decompose into the elements rather than form under relevant conditions. However, assuming that Cr is already constituent part in Cr_2O_3 before first contact with Pb–16Li, the calculations suggest a very low oxygen concentration required for formation of ternary $LiCrO_2$, by several orders of magnitude lower than oxygen solubility (Fig. 5). This may explain why Cr, or better put almost inevitable Cr_2O_3 on the surface of solid Cr, rapidly getters oxygen from Pb–16Li [35], whereas neither Cr_2O_3 nor $LiCrO_2$ are thermodynamically stable [15]. However, the effect can be only temporary, as $LiCrO_2$ subsequently tends to dissolve. It should be noted that this findings from thermodynamic calculations will not change qualitatively if other numbers are assumed for oxygen solubility.

In Fig. 5, also oxygen solubility calculated by Buxbaum [36] (Eq. (18) is depicted, suggesting that 3 µg/g dissolved oxygen as assumed by Lyublinski et al. [23] in order to demonstrate the oxygen influence on the saturation concentrations of Fe or Cr are relevant only if the comparatively high oxygen solubility inferred by Buxbaum actually applies. But this does not necessarily compromise their qualitative result, i.e., that dissolved oxygen tends to increase the saturation concentration of dissolved Cr, in contrast to Fe.

4.5. Diffusivity in Pb–16Li

As introduced above, diffusion in Pb–16Li may become the rate determining step in solution, e.g. across the diffusion boundary layer in flowing Pb–16Li [38]. In their experimental study performed at 500 °C, Simon et al. [12] find $D_{Fe} = 4\ (\pm 2) \times 10^{-14}$ m^2/s and $D_{Cr} = 8\ (\pm 2.5) \times 10^{-11}$ m^2/s for diffusivity of Fe and Cr, respectively. Accordingly, for similar concentration gradient, Cr would diffuse faster than Fe. Fe diffusivity suggested for Pb–16Li is about 10^4 times lower than reported by Robertson [39] for Fe diffusion in pure liquid Pb at the same temperature (5×10^{-10} m^2/s). The quite significant difference in Fe and Cr diffusivity is in contrast to the similar atom radius of the two elements (Stokes–Einstein equation).

Feuerstein [20] observes $D_{Fe} = 7.48 \times 10^{-11}$ and 1.14×10^{-10} m^2/s at 500 and 600 °C, respectively, which is closer to but still an order of magnitude lower than diffusivity in Pb found by Robertson [39]. This Fe diffusivity approaches the Cr diffusivity determined by Simon et al. [12]. The corresponding Arrhenius function [20] is

$$\ln D_{Fe} = -19.64 - 2844/T \quad (19)$$

with D_{Fe} and T in m^2/s and K, respectively. Feuerstein [20] also reports V diffusivity in Pb–16Li given by

$$\ln D_V = -25.7 + 2300/T \quad (20)$$

(D_V – V diffusivity in m^2/s; T – temperature in K). Eq. (20) may be best understood as average 1.5×10^{-10} m^2/s between 400 and 600 °C.

A possible influence of dissolved oxygen on diffusivity of the metals has not yet been taken into account, nor is information about oxygen concentration in their experimental measurement available.

5. EUROFER97 in Pb-16Li

As discussed above, steel corrosion in Pb–16Li is mainly caused by dissolution of the steel constituents (selective or non-selective), which consists of atom transfer across the solid/liquid interface and diffusion (transport from the solid/liquid interface into the volume of the liquid metal) supported by convection in the liquid. Experimental observations suggest an incubation time of the dissolution process, which, in the case of EUROFER, is about 1000 h [40–42]. During this time, the degradation of surface oxides takes place, oxides primarily of iron or chromium. These naturally form in the course of sample preparation, handling or

storage, but may also be deliberately produced before the exposure to the liquid metal. While the steel composition immediately underneath these oxides is unlikely to change when formed at rather low temperature, depletion in the element(s) that enriches in the oxide is typical for (pre-)oxidation at high temperature.

In general, 2000 h seem to be sufficient to observe the effects of dissolution in EUROFER, at least locally, though this may, finally, depend on temperature or other conditions. Observations as to the selectivity of the dissolution process for either of the major elements in the steel, namely Fe or Cr, are not unanimously, as touched already above, in connection with Cr solubility in Pb–16Li. If selectivity is reported for EUROFER [28,32], it typically is Cr that preferentially leaves the steel. In addition to a zone clearly depleted in Cr (~1 μm after 4500 h at 480 °C), which detaches when being undercut by the liquid metal, porosity may develop between the Cr-depleted portion and the bulk of the steel [28], most likely along grain boundaries. The explanation offered by the authors is based upon Cr solubility in Pb–16Li being lower but diffusivity higher than for Fe [28]. However, Fe solubility may, finally, be not as high and diffusivity not as low as they assume (see Sections 4.1 and 4.5). Assuming, in general, quite similar Fe and Cr solubility or diffusivity in Pb–16Li, dissolved oxygen can make a difference in the capacity of the liquid metal for absorbing these elements (see Section 4.2), i.e. Cr depletion tends to increase with increasing concentration of oxygen in Pb–16Li such as observed for austenitic steel at 600 °C [33]. Irrespective of this effect of oxygen being linked to the formation of $LiCrO_2$ [33], which is in contrast to the estimated thermodynamic stability of this oxide (Fig. 5 and related discussion), or the result of some weaker association of Cr and oxygen atoms in Pb–16Li, it may explain why, at same temperature, Cr depletion in EUROFER is observed in some experiments but not in others. While operating oxygen sensors in Pb–16Li was tried [43], oxygen monitoring has not yet become common practice for materials testing in this liquid metal.

Apart from the anticipated effect of dissolved oxygen on the ratio of Fe and Cr dissolution, general factors of influence on corrosion of EUROFER caused by Pb–16Li are the temperature of exposure and flow velocity. In static liquid metal, the ratio of area of steel surface exposed and available volume of liquid metal is the parameter alternative to flow velocity. However, in view of corrosion mass transfer (Table 2 and related discussion) and its repercussions for the rate of element dissolution, the size of the system, i.e., mass flow, also plays a role in the case of flowing liquid metal, just as temperature gradients that exist under both flowing and static conditions. As for exposure time, experimental observations for flowing Pb–16Li [40,41,44–46] suggest that corrosion of EUROFER, in terms of loss of cross section, either diameter or area-specific mass, increases linearly with time once the incubation period has passed. Such linear progress as a function of time is typical for dissolution in a non-saturable liquid and allows of estimating a valid corrosion rate (μm/y) after any duration of exposure longer than incubation. If the latter cannot explicitly be considered, the calculated corrosion rate is likely to reflect the situation the more precisely the longer the exposure time after which it was determined.

Data on corrosion of EUROFER97 in flowing Pb–16Li is summarized in Table 3. In the corresponding experiments, the flow velocity varies from 0.01 to 0.3 m/s, temperature is 480 or 550 °C, and maximum exposure time about 12 000 h (1.4 years). The best part of these corrosion tests was performed in the identical experimental device, namely the PICOLO loop being operated at KIT [40,44–47],with same relation between flow velocity and mass flow and similar minimum temperature along the loop. Especially in these tests performed in PICOLO depletion of EUROFER in either Cr or Fe does not occur, or occurs at a level not noticeable (<1 μm) in the scanning electron microscope (SEM) supplemented by energy-dispersive X-ray microanalyses (EDS). The crosscheck on a EUROFER sample from a recent exposure campaign in PICOLO at 550 °C (Fig. 6) also reveals no clear (Cr-) depletion of the near-surface portion of the steel, though the intensity ratio of X-rays emitted by Cr and Fe is, on average, slightly lower in the first 2–3 μm at the surface in comparison to the bulk of the steel. Incubation time seems to be a function of temperature rather than flow velocity [45].

At flow velocity 0.3 m/s (Table 3), observed corrosion rate at 480 and 550 °C is 90 and 700 μm, respectively, so that Arrhenius analysis suggests an apparent activation energy $E = 151$ kJ/mol. Assuming that element transport through the diffusion boundary layer was the rate-determining step of the corrosion process, Eqs. (6) (with $c_{s/l} = S$) and 7 imply $E > 5/6\ E_D$ (E_D – activation energy of diffusion) because the solubility S (or rather, the solubility reduced by a factor depending on steel composition [48]) of the diffusing elements generally increases

Table 3
Data on corrosion of EUROFER97 in flowing Pb–16Li.

Ref.	Flow velocity of lead–lithium, (m/s)	Temperature (°C)	Duration of exposure (h)	Corrosion rate, μm/y
[28]	10^{-2}	480	4500	40
[40,48]	0.3	480	12 000	90
[48]	0.3	550	12 320	700
[44]	0.22	550	12 000	400
[45]	0.1	550	3000	300
[46]	0.1	550	12 000	220

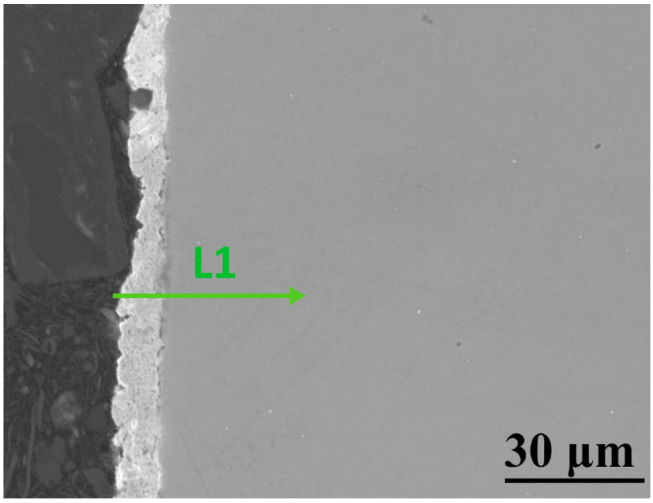

(a)

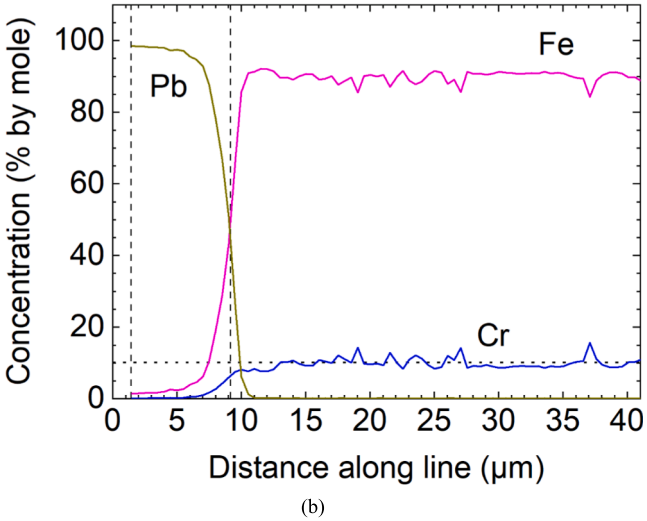

(b)

Fig. 6. (a) SEM micrograph of EUROFER97 after exposure for 3000 h to flowing Pb–16Li in the PICOLO loop at 550 °C and (b) results from EDS analyses performed along the line indicated in (a).

with increasing temperature. For diffusion of Fe in Pb–16Li, with activation energy following from Eq. (19) as 342 kJ/mol, or 5/6 E_D = 285 kJ/mol, the criterion is not met. However, this should not yet mean that diffusion of Fe or another steel element in the liquid metal cannot be the rate-determining step of the dissolution of EUROFER, it may at this stage just reflect that available data, especially for diffusion in Pb–16Li, is not accurate enough for such quantitative analysis of corrosion data. Another approach to analyzing whether the corrosion rates observed for EUROFER comply with diffusion control is plotting the data in Table 3 as a function of the square root of the flow velocity u_0, what has been done in Fig. 7. Evaluable in more detail is only the data set for 550 °C, which consists of more than two points. The dependence on $u_0^{½}$ is linear as predicted by combining Eqs. (6) and (7). The resulting straight line does not intersect the ordinate at $u_0^{½} = 0$, but zero corrosion is approached at about 0.2 $m^{½}/s^{½}$ or a flow velocity of 0.04 m/s. The linear relationship losing validity for $u_0 \to 0$ formally follows from Eq. (7), in that an infinitely thick diffusion boundary layer would result. On the other hand, corrosion will generally not vanish at $u_0 = 0$ but attain a certain value that should largely depend on the volume of static liquid metal that is present [32]. Likewise, the corresponding mass flow may be decisive for down to which flow velocity such a linear relationship applies. The increase in the corrosion rate at 550 °C for flow velocity increasing from 0.1 to 0.3 m/s is factor 2.6, in contrast to 2.25 at 480 °C and 10^{-2} to 0.3 m/s. In the light of diffusion control, this suggests that in the considered range of flow velocity and temperature, the effect of temperature, i.e., thermal activation of diffusion and likewise exponential increase with increasing temperature of solubility in the liquid metal, outweighs the diffusion boundary layer and mass flow becoming thinner and larger, respectively, (steeper concentration gradient) with increasing flow velocity. At the end of this analysis of corrosion data it should be emphasized that in the absence of appreciable element depletion in the steel, such as in the tests performed in PICOLO, the possible rate-determining steps of dissolution are confined to atom transfer across the solid/liquid interface, transport in the diffusion boundary layer or convection with the liquid–metal flow. Especially the observed dependence of corrosion rate on flow velocity suggests diffusion being rate-determining, where the element removal from the solid/liquid interface occurs largely in proportion to the steel composition.

If experimental results on plain corrosion of EUROFER97 are scarce, information on the impact of Pb–16Li on the mechanical properties of the steel is even scarcer. Tensile properties at 480 °C remain largely unaltered after exposure for up 4500 h to flowing Pb–16Li at the same temperature [28]. Slow-strain-rate tensile tests performed in static Pb–16Li at 250–400 °C equally show no detrimental effect of the presence of the liquid metal [49], however, with pre-exposure to the liquid metal for 30 min, which could have been too short to destroy surface oxides on the tested samples. Subsequent tests with pre-exposure to Pb–16Li at 470 °C for 1000 h show a decrease in total elongation (partial loss of ductility), whereas yield or tensile strength largely remain unaltered [50]. However, loss in ductility may be almost complete if a significant surface defect such as a notch [50] is present in the steel. Tensile tests performed after neutron irradiation at about 300 °C of EUROFER in contact with Pb–16Li point at irradiation hardening but are unsuspicious as to an effect of the liquid metal [51]. As for dissolution of EUROFER caused by static Pb–16Li, neutron irradiation possibly promotes the development of porosity in the steel, near the steel surface. [52], however, as already mentioned above, that may be observed also in the absence of neutrons [28].

For magnetic-confinement fusion, additionally, the influence of the magnetic field on interactions between EUROFER and Pb–16Li is of some importance. Experiments in flowing (0.05 m/s) Pb–16Li at 515 and 550 °C [53] reveal that inside a magnetic field of 1.8 T, the corroding surface develops a periodic wavy structure. Dissolution of EUROFER is clearly faster than outside the magnetic field. Indicative average dissolution rates at 515 °C are 330 and 150 μm/y inside and outside the magnetic field, respectively. Corresponding numbers for 550 °C are 820 and 410 μm. The waviness of the solid/liquid interface as well as acceleration of dissolution are likely to result from the action of the magnetic field on the liquid–metal flow [54]. It should be noted here that corrosion rates found outside the magnetic field are somewhat higher than data in Table 3 would suggest for flow velocity 0.05 m/s. This discrepancy is indicative of the influence of the particular testing facility on the results obtained for nominally same exposure conditions. Sample geometry or evaluation procedure may also play a role.

6. Other RAFM or martensitic steels

Fig. 8 compares material loss in different RAFM steels with nominally 9 % (by mass) Cr that is observed after exposure to flowing (0.1 m/s) Pb–16Li at 550 °C in the identical experimental facility (PICOLO) [40,44–47,55]. The quantitative results seem to be largely interchangeable, despite more or less pronounced differences in microstructure of the steels or minor element concentration. This implies that gaps in quantitative data existing for one may be closed by corrosion rates observed for others, however, keeping always in mind a potential influence of the particular testing facility. By their analysis of corrosion rates for ferritic/martensitic steels with Cr content around 9 % exposed to flowing Pb–16Li in different facilities, Sannier et al. [38] arrive at

$$r = 8 \times 10^{9} exp(-12975/T) u^{0.875} d^{-0.125} \quad (21)$$

(r – corrosion rate in μm y^{-1}; T – temperature in K; u – flow velocity of

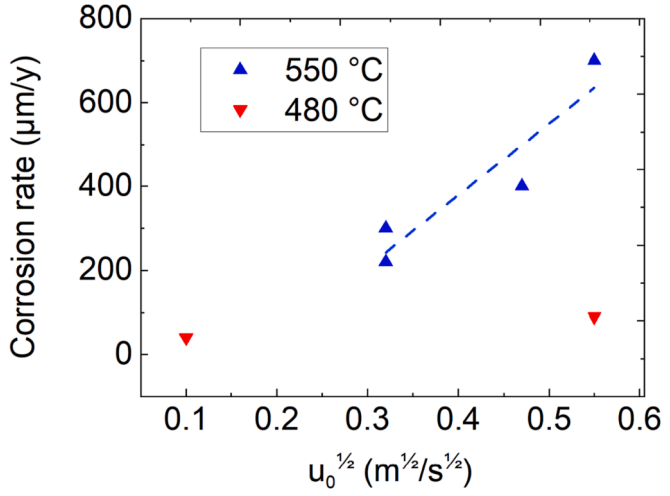

Fig. 7. Corrosion rate of EUROFER97 [28,40,44–46,48] vs. square root of flow velocity for exposure to flowing Pb–16Li at 480 and 550 °C.

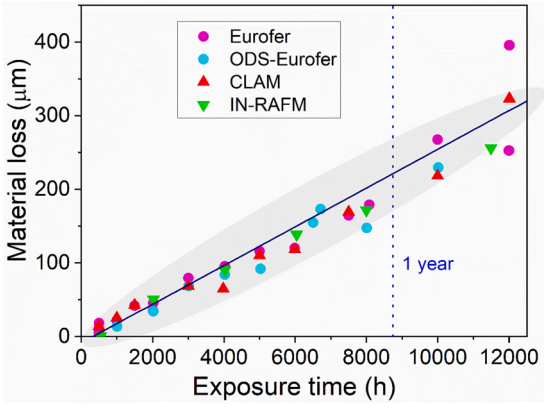

Fig. 8. Comparison of the average material loss (surface recession) for RAFM steels after exposure to flowing Pb–16Li at 550 °C and 0.1 m/s [40,44–48].

Pb–16Li in m/s; d – characteristic diameter in m). As the underlying corrosion data includes experimental set-ups in which cylindrical test samples (on which the corrosion rate was determined) reside in a vertical test-section tube of the facility, it is not immediately clear from the analysis whether u is the nominal velocity of the test, typically the one in the annular gap between sample and inner tube wall, or the velocity in the empty tube. Similar uncertainty remains with respect to the diameter d, whether e.g., the hydraulic diameter of the annular gap or inner diameter of the empty tube. Example calculations for the PICOLO loop (16 and 8 mm inner tube and sample diameter, respectively) at 550 °C and 0.3 m/s yield 794 μm/y if the hydraulic situation around the samples is considered, in contrast to 519 μm/y resulting for inserting the empty-tube velocity and inner tube diameter into Eq. (21). Correspondence to 700 μm/y as found experimentally (Table 3) is fairly good if nominal flow velocity and hydraulic diameter of the annular gap between sample and tube wall are being used. For 0.22 m/s with experimental corrosion rate of 400 μm/y (Table 3), inserting the empty-tube values into Eq.21 (395 μm/y) gives the better result, whereas the observed rate is overpredicted by about 50 % otherwise (605 μm/y). It so far seems that Eq. (21) at least approximates the corrosion rate of (9 % Cr) ferritic martensitic steels in flowing Pb–16Li, with the limitations as to predictive power when flow velocity falls below a certain value (Fig. 7 and related discussion). It should, however, be noted that the exponents of u and d in this equation follow from the assumption that element diffusion dominates mass transport across the laminar boundary layer [38] rather than the diffusion boundary layer(s). In liquid metals, the latter is actually thinner (see Section 3) so that concentration gradients at the solid/liquid interface are steeper than here assumed. While the conditions for disproportionate transfer of Cr to Pb–16Li still need to be better understood, the selective leaching of this element, if occurring, has some impact on element enrichment in the liquid metal, subsequent reprecipitation in the presence of temperature gradients. An approach to the quantitative assessment of this phenomenon as observed for the Indian RAFM is proposed by Chakraborty et al. [56].

Additional input from tests on other steels is especially valuable where experimental results for EUROFER97 are relatively scarce, e.g., the impact of Pb–16Li on the mechanical properties, influence of strong magnetic fields or neutron irradiation on the interaction with the liquid metal. As for the former, tensile tests at 250 or 400 °C in Pb–16Li indicate no loss of ductility in F82H-mod. or OPTIFER IVb, except for the heat-affected zone in welded material at 250 °C. Specific post-weld heat-treatment restores the properties of these RAFM steels with nominally 8 and 9 % Cr, respectively [57]. Before these tests, pre-exposure to Pb–16Li in order to destroy surface oxide is performed at 500 °C for 15 h, clearly shorter than, though at higher temperature as in tests that show a degradation of mechanical properties for EUROFER (470 °C, 1000 h) [50]. Sun et al. [58] find a partial loss in ductility of 9 Cr RAFM steel CLF-1 especially after exposure for 1500 h to flowing Pb–16Li at 400 °C when static mechanical stress (250 MPa) was simultaneously applied. Ageing under stress results in only intermittently reduced strength (500 h). Ductility is retained in the presence of the liquid metal at 300 and 350 °C. Exposure for 1000 h to flowing Pb–16Li at 550 °C, in a magnetic field of 1.7 T leaves the room-temperature tensile properties for 9 Cr martensitic steel T91 largely unaltered [59].

For 12 Cr martensitic steel, Borgstedt and Grundmann [60] do not observe a clear reduction in tensile properties caused by Pb–16Li at 240 or 300 °C after pre-exposure to the liquid metal at 550 °C for up to 1500 h. Their stress-rupture tests in Pb–16Li show an only slight reduction in stress-rupture life, which rather may be attributed to the reduction of load-bearing cross section as a result of simultaneous dissolution of the steel [61]. Low-cycle fatigue tests in Pb–16Li performed on this steel at 550 °C by the same group point at a reduction in fatigue life especially after pre-exposure for 1000 h [61]. Accompanying corrosion tests in flowing Pb–16Li suggest that the incubation of dissolution may take longer for the 12 Cr steel than for EUROFER.

7. Conclusions

The question of EUROFER97 being compatible with Pb–16Li, e.g., damage in the steel, anticipated for a given service situation, being tolerable at the end of the design lifetime, may at this stage be answered primarily under consideration of the dissolution of the steel. Observed dissolution rate of 700 μm/y at nominally 550 °C and 0.3 m/s flowing Pb–16Li seems to be on the critical side, whereas 90 and 220 μm/y indicated for exposure at lower temperature (480 °C) and flow velocity (0.1 m/s), respectively, could be judged sufficiently low. It should, however, be noted that not only the loss in material but also the related transfer of steel elements to the liquid metal, corrosion mass transfer, must not exceed a limit predefined for the application. Strong magnetic fields as typical for magnetic-confinement fusion generally accelerate steel dissolution.

The degradation of EUROFER beyond dissolution such as the partial loss in ductility is linked to the incubation of steel dissolution, i.e., dissociation of surface oxide and intimate contact of liquid metal and steel are likely to be required. Surface defects in the steel may play a role for the degree of loss in ductility, which finally must also comply with some limits given by the case of application. As for the interference of neutron irradiation, the very limited data that could be evaluated does not yet point at a clear detrimental effect on the liquid–metal/steel interactions. Besides natural surface oxide, oxygen dissolved in Pb–16Li is likely to influence corrosion, notably the ratio of Fe and Cr transfer from the steel to the liquid metal.

The gaps for a complete compatibility assessment largely consist in confirmed data related to the influence of Pb–16Li exposure on the mechanical properties of EUROFER and, with view to thermonuclear fusion, the impact of neutron irradiation. The dissolution of EUROFER is comparatively well characterized, except for the reason of Cr depletion being sometimes observed, sometimes not. Dissolution theory helps in transferring experimental observations to other conditions, though for doing so, more reliable data on element solubility and diffusivity in Pb–16Li seems to be required. Characterizing experimental conditions by a Reynolds number instead of flow velocity, alternatively by both flow velocity and mass flow, as well as monitoring of oxygen dissolved in Pb–16Li is suggested for qualifying tests in the future.

Declaration of Competing Interest

The authors declare that they have no known competing financial interests or personal relationships that could have appeared to influence the work reported in this paper.

Data availability

The data that has been used will be made available on request.

Acknowledgements

Many of the studies evaluated in this survey were carried out within the framework of the EUROfusion Consortium and received funding from various Euratom research and training programs. The views and opinions expressed herein do not necessarily reflect those of the European Commission. The authors gratefully acknowledge additional funding of their work by the Helmholtz Program FUSION as well as the Helmholtz Initiative for Refugees.

References

[1] R. Lindau, et al., Present development status of EUROFER and ODS-EUROFER for application in blanket concepts, Fusion Eng. Des. 75–79 (2005) 989–996.
[2] L.M. Giancarli, et al., Overview of recent ITER TBM Program activities, Fusion Eng. Des. 158 (2020), 111674.
[3] O.K. Chopra, D.L. Smith, P.F. Tortorelli, J.H. DeVan, D.K. Sze, Liquid-metal corrosion, Fusion Technol. 8 (1985) 1956–1969.

[4] J. Luo, H. Cheng, K.M. Asl, C.J. Kiely, M.P. Harmer, The role of a bilayer interfacial phase on liquid metal embrittlement, Science 1979 (333) (2011) 1730–1733.
[5] V.V. Popovich, I.G. Dmukhovskaya, Rebinder effect in the fracture of Armco iron in liquid metals, Mater. Sci. 14 (1978) 365–370.
[6] C.F. Old, Liquid metal embrittlement of nuclear materials, J. Nucl. Mater. 92 (1980) 2–25.
[7] K. Wolski, V. Laporte, Grain boundary diffusion and wetting in the analysis of intergranular penetration, Mater. Sci. Eng. A 495 (2008) 138–146.
[8] L.F. Epstein, Static and dynamic corrosion and mass transfer in liquid metal system, Chem. Eng. Prog. 53 (1957) 67–81.
[9] de S. Brasunas, A., Liquid metal corrosion, Corrosion 9 (1953) 78–84.
[10] C. Schroer, O. Wedemeyer, J. Novotny, A. Skrypnik, J. Konys, Selective leaching of nickel and chromium from Type 316 austenitic steel in oxygen-containing lead-bismuth eutectic (LBE), Corros. Sci. 84 (2014) 113–124.
[11] V.G. Levich, Physicochemical hydrodynamics, Prentice Hall, 1962.
[12] N. Simon, T. Flament, A. Terlain, Determination of the diffusion coefficients of iron and chromium in Pb17Li, Int. J. Heat Mass Transf. 38 (1995) 3085–3090.
[13] M. Hansen, K. Anderko, H.W. Salzberg, Constitution of binary alloys, J. Electrochem. Soc. 105 (1958) 260C.
[14] A.K. Niessen, et al., Model predictions for the enthalpy of formation of transition metal alloys II, Calphad 7 (1983) 51–70.
[15] P. Hubberstey, Pb-17Li and lithium: A thermodynamic rationalisation of their radically different chemistry, J. Nucl. Mater. 247 (1997) 208–214.
[16] F.J. Smith, The solubilities of thorium and samarium in liquid lithium-lead solutions, J. Less-Common Met. 32 (1973) 297–300.
[17] M.G. Barker, T. Sample, The solubilities of nickel, manganese and chromium in Pb-17Li, Fusion Eng. Des. 14 (1991) 219–226.
[18] V. Coen, T. Sample, Pb-17Li: A fully characterised liquid breeder, Fusion Technol. 1990 (1991) 248–252.
[19] H.U. Borgstedt, H. Feuerstein, The solubility of metals in Pb-17Li liquid alloy, J. Nucl. Mater. 191–194 (1992) 988–991.
[20] H. Feuerstein, et al., Compatibility of 31 metals, alloys and coatings with static Pb-17Li eutectic mixture, Forschungszentrum Karlsruhe GmbH (1995).
[21] D.A. Stevenson, J. Wulff, Liquid-solid phase distribution studies, Trans. Met. Soc. AIME 221 (1961) 271.
[22] M. Kondo, et al., Metallurgical study on corrosion of RAFM steel JLF-1 in Pb-Li alloys with various Li concentrations, Fusion Eng. Des. 125 (2017) 316–325.
[23] I.E. Lyublinski, V.A. Evtikhin, V.Y. Pankratov, V.P. Krasin, Numerical and experimental determination of metallic solubilities in liquid lithium, lithium-containing nonmetallic impurities, lead and lead-lithium eutectic, J. Nucl. Mater. 224 (1995) 288–292.
[24] A.R. Miedema, The electronegativity parameter for transition metals: heat of formation and charge transfer in alloys, J. Less-Common Met. 32 (1973) 117–136.
[25] F. Balbaud-C El Erier, F. Barbier, Investigation of models to predict the corrosion of steels in flowing liquid lead alloys, J. Nucl. Mater. 289 (2001) 227–242.
[26] T. Alden, D.A. Stevenson, J. Wulff, Solubility of nickel and chromium, Trans. Metall. Soc. AIME 1 (1958) 15–17.
[27] N. Simon, A. Terlain, T. Flament, The compatibility of martensitic steels with liquid Pb – 17Li, J. Nucl. Mater. 254 (1998) 185–190.
[28] G. Benamati, C. Fazio, I. Ricapito, Mechanical and corrosion behaviour of EUROFER 97 steel exposed to Pb-17Li, J. Nucl. Mater. 307–311 (2002) 1391–1395.
[29] Y. Chen, et al., Corrosion analysis of CLAM steel in flowing liquid LiPb at 480 °c, Fusion Eng. Des. 85 (2010) 1909–1912.
[30] P. Chakraborty, et al., Corrosion of Indian RAFMS in Pb-17Li in a rotating disc corrosion test facility at 773 K, Fusion Eng. Des. 100 (2015) 181–189.
[31] X. Chen, Q. Yuan, B. Madigan, W. Xue, Long-term corrosion behavior of martensitic steel welds in static molten Pb-17Li alloy at 550°C, Corros. Sci. 96 (2015) 178–185.
[32] S. Bassini, V. Cuzzola, A. Antonelli, M. Utili, Long-term corrosion behavior of EUROFER RAFM steel in static liquid Pb-16Li at 550 °C, Fusion Eng. Des. 160 (2020), 111829.
[33] M.G. Barker, et al., Effect of oxygen impurities behaviour of type 316 stainless steel in Pb-17Li, J. Nucl. Mater. 155–157 (1988) 732–735.
[34] B.E. Pelzel, Solubility of Tellurium, Selenium and Manganese in liquid lead, Metall 10 (1956) 717–719.
[35] M.G. Barker, J.A. Lees, T. Sample, Determination of the solubility of oxygen in Pb-17Li. in *Proc. of the 4th Int. Conf. on Liquid Metal Engineering and Technology* vol. 1 206(1)-206(8) (Proc. 4th In t. Conf. on Liq. Met. Eng. and Tech n o l., 1988).
[36] R.E. Buxbaum, A chemical theory analysis of the solution thermodynamics of oxygen, nitrogen and hydrogen in lead-rich LiPb mixtures, J. Less-Common Met. 97 (1984) 27–38.
[37] W.R. Smith, Computer software reviews HSC Chemistry for Windows 2 (1995).
[38] J. Sannier, T. Flament, A. Terlain, Corrosion of martensitic steels in flowing Pbl7Li, Fusion Technol. 1990 (1991) 901–905.
[39] W.M. Robertson, Diffusion of cobalt and iron in liquid lead measured by grain boundary grooving, Trans. TMS-AIME 242 (1968) 2139.
[40] J. Konys, W. Krauss, Z. Voss, O. Wedemeyer, Corrosion behavior of EUROFER steel in flowing eutectic Pb-17Li alloy, J. Nucl. Mater. 329–333 (2004) 1379–1383.
[41] K. Splíchal, M. Zmítko, Corrosion behaviour of EUROFER in Pb-17Li at 500 °C, J. Nucl. Mater. 329–333 (2004) 1384–1387.
[42] H. Glasbrenner, J. Konys, Z. Voß, Corrosion behaviour of low activation steels in flowing Pb-17Li, J. Nucl. Mater. 281 (2000) 225–230.
[43] N.P. Bhat, H.U. Borgstedt, Oxygen in the liquid-metal fusion reactor blanket and its possible influence on the compatibility with materials, Fusion Technol. 21 (1992) 52–59.
[44] J. Konys, et al., Compatibility behavior of EUROFER steel in flowing Pb-17Li, J. Nucl. Mater. 386–388 (2009) 678–681.
[45] J. Konys, W. Krauss, H. Steiner, J. Novotny, A. Skrypnik, Flow rate dependent corrosion behavior of Eurofer steel in Pb-15.7Li, J. Nucl. Mater. 417 (2011) 1191–1194.
[46] J. Konys, W. Krauss, Z. Zhu, Q. Huang, Comparison of corrosion behavior of EUROFER and CLAM steels in flowing Pb-15.7Li, J. Nucl. Mater. 455 (2014) 491–495.
[47] W. Krauss, S.E. Wulf, J. Konys, Long-term corrosion behavior of ODS-Eurofer in flowing Pb-15.7Li at 550 °C, Nucl. Mater. Energy 9 (2016) 512–518.
[48] C. Schroer, Dissimilar metal solution from solid alloys as observed for steels and nickel-based alloys in the presence of lead-based liquid alloys or liquid tin, JOM 73 (2021) 4000–4008.
[49] R.W. Bosch, S. van Dyck, A. Al Mazouzi, Investigation of the susceptibility of EUROFER97 in lead-lithium to liquid metal embrittlement (LME), Fusion Eng. Des. 82 (2007) 2615–2620.
[50] J. Van den Bosch, R.W. Bosch, D. Sapundjiev, A. Almazouzi, Liquid metal embrittlement susceptibility of ferritic-martensitic steel in liquid lead alloys, J. Nucl. Mater. 376 (2008) 322–329.
[51] A. Aiello, G. Benamati, R. Melder, A. Povstyanko, Mechanical properties of Eurofer 97 in Pb-16Li and irradiation effect, J. Nucl. Mater. 376 (2008) 396–400.
[52] K. Splichal, J. Berka, M. Zmitko, L. Viererbl, Z. Lahodova, Interaction of Pb -16Li melt with EUROFER97 under higher temperature and neutron irradiation, Fusion Eng. Des. 126 (2018) 73–78.
[53] R. Krishbergs, et al., Experimental studies of the strong magnetic field action of the corrosion of RAFM steels in Pb17Li melt flows, Magnetohydrodynamics 45 (2009) 289–296.
[54] I. Bucenieks, et al., Investigation of corrosion phenomena in EUROFER steel in Pb-17Li stationary flow exposed to a magnetic field, Magnetohydrodynamics 42 (2006) 237–251.
[55] J. Konys, W. Krauss, Z. Voss, O. Wedemeyer, Comparison of corrosion behavior of bare and hot-dip coated EUROFER steel in flowing Pb-17Li, J. Nucl. Mater. 367–370 (2007) 1144–1149.
[56] P. Chakraborty, V. Singh, S. Bysakh, R. Tewari, V. Kain, Short-term corrosion behavior of Indian RAFM steel in liquid Pb-Li: Corrosion mechanism and effect of alloying elements, J. Nucl. Mater. 520 (2019) 208–217.
[57] T. Sample, H. Kolbe, Liquid metal embrittlement (LME) susceptibility of the 8–9% Cr martensitic steels F82H-mod., OPTIFER IVb and their simulated welded structures in liquid Pb-17Li, J. Nucl. Mater. 283–287 (2000) 1336–1340.
[58] Z. Sun, et al., Effect of applied stress on the ductility of RAFM steel during long-term exposure in flowing Pb-17Li, Fusion Eng. Des. 192 (2023), 113640.
[59] E. Platacis, et al., Investigation of the Li-Pb flow corrosion attack on the surface of P91 steel in the presence of magnetic field, Magnetohydrodynamics 48 (2012) 343–350.
[60] H.U. Borgstedt, M. Grundmann, The influence of liquid Pb-17Li eutectic on the mechanical properties of structural materials, Fusion Eng. Des. 6 (1988) 155–158.
[61] H.U. Borgstedt, G. Frees, M. Grundmann, Z. Peric, Corrosion and mechanical properties of the martensitic steel X18CrMoVNb 12 1 in flowing Pb-17Li, Fusion Eng. Des. 14 (1991) 329–334.